Experimental Determination of Crack-Face Interference-Free Mode I and Mode II Crack Propagation Behaviour of Normalized SAE 1045 Steel.

John J.F. Bonnen[1] **and Timothy H. Topper**[2]

[1]Research Staff, Ford Motor Co., MD3135 RIC, P.O.B. 2053, Dearborn, MI, 48121 USA
[2]Department of Civil Eng., University of Waterloo, Waterloo, Ontario, Canada, N2L 3G1

ABSTRACT. *A series of unique long crack da/dN-delta K experiments that employed periodic overloads to eliminate crack closure were used to determine both the mode I and the mode II crack closure-free crack propagation behavior of normalized SAE 1045 steel. A good correlation was found between the mode I and mode II crack growth rate curves. Similarly, there was a good correlation between short crack growth rate data taken from the literature and the present crack closure-free long crack data. Short and long crack data for all of the modes fall into a single scatter band, and the threshold stress intensity is about the same for all the data sets.*

INTRODUCTION

In the early 1970's Elber [1, 2] demonstrated that crack closure substantially reduces the mode I crack driving force seen at the crack tip, and a similar concept, crack-face interference, has extended this idea to include modes II and III. In this paper we present crack-face interference-free long crack testing techniques and the resulting crack growth rate data for both modes I and II crack growth.

Although eliminating crack-face interference is difficult to achieve, two techniques have been successfully used to achieve this – the application of sufficiently large constant tensile stresses normal to the crack face [3, 4, 5, 6] (under mode I loading this means very high mean stresses) and the periodic insertion into a constant amplitude stress history of very large overloads (on the order of the net section yield stress) either normal to [5, 7] or in the plane of the growing crack [5, 8, 9]. The first technique keeps the crack faces apart, and the second technique, depending on how it is employed, keeps the crack faces apart and/or crushes existing crack face asperities flat so that they no longer hinder crack growth. Once crack-face interference has been eliminated we obtain the most conservative possible fatigue crack growth rate curve for a given material.

In this paper these techniques and the unique properties of this particular steel are used by the present authors to develop not only a mode I crack closure free (or effective) long crack crack growth curve but also a mode II long crack crack-face interference-free crack propagation curve for normalized SAE 1045 steel.

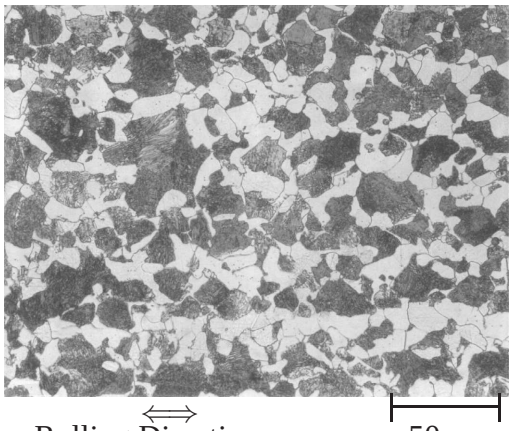

Figure 1. Microstructure of normalized SAE 1045 steel (400X), L-T orientation. Note longitudinal banding of ferrite and pearlite.

Table 1. Mechanical Properties of normalized SAE 1045.

Hardness	203 BHN		Yield Stress, Upper	476MPa
Engin. Failure Strain, e_f	0.432		Yield Stress, Lower	397MPa
Strength Coef., K	1370MPa		Ult. Stress	703MPa
Strain Hardening Exp., n	0.261		Young's Modulus, E	203GPa
Cyclic Properties				
Yield Stress, prop. limit	155MPa		Fat. Strength Coef., σ'_f	1580MPa
Yield Stress, 0.2% Offset	379MPa		Fat. Strength Exp., b	-0.136
Cyc. Strength Coef., K'	1480MPa		Fat. Duct. Coef., ε'_f	0.733
Cyc. Strain Hard. Exp., n'	0.221		Fat. Duct. Coef., c	-0.566

MATERIALS AND PROCEDURES

In this investigation a normalized SAE 1045 steel with a nominal hardness of 203 BHN, previously the focus of an SAE Fatigue Design and Evaluation Committee multiaxial fatigue study [10, 11], was used in both crack growth and fatigue life experiments. The steel had a ferritic-pearlitic microstructure which was moderately banded longitudinally resulting in ferrite-rich and poor channels, as can be seen in Figure 1. The grains are roughly equiaxed and average $25\mu m$ in diameter. Mechanical properties are listed in Table 1.

The biaxial tubular crack growth specimen of Figure 2, has a central 0.25mm diameter hole from which a precrack was grown. The Single Edge Notched (SEN) specimen pictured in Figure 3 has a similar sized notch for the precrack, and it was used to determine the mode I crack closure free crack growth behavior of the material. Both crack growth specimens were given a final longitudinal $5\mu m$ polish. All crack growth testing was conducted using computer control at frequencies ranging from 1-40Hz for biaxial specimens and 1-100Hz for axial specimens.

The SEN specimens were rigidly bolted into the grips so that no rotation about the holes was possible. A 45kN axial servohydraulic load frame was used for these tests.

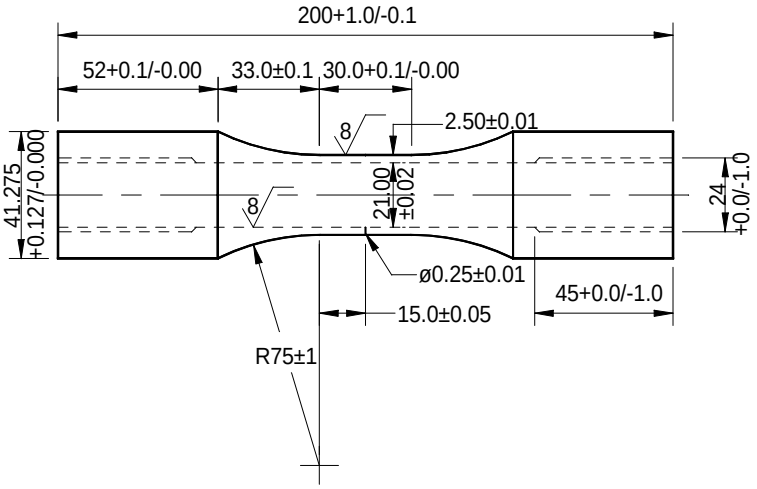

Figure 2. Tubular crack growth specimen. All dimensions in mm.

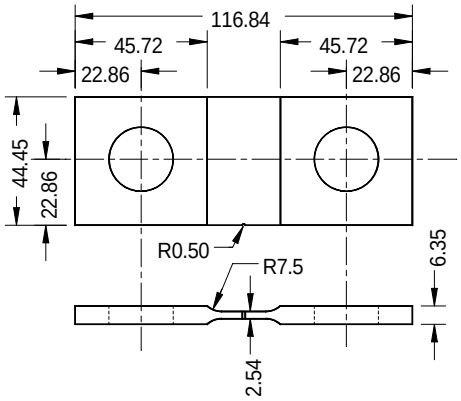

Figure 3. Specimen used for mode I crack growth testing. All dimensions in mm.

Specimens were precracked to a total crack length of 2.5mm using a fully reversed constant amplitude nominal stress of 276MPa. Crack growth measurements made below ΔK=10MPa$\sqrt{\text{m}}$ were taken using a high R-ratio loading cycle such as found that in Figure 4a. Above that level a periodic overload history with a fully reversed overload cycle of 276MPa was used, as in Figure 4b. Only in those cases where the required stress intensity range caused the small cycle minimum to approach that of the overload was the size of the overall overload cycle increased. Crack length measurements were made using a 900x long focal length microscope that allowed crack length to be determined to within $2\mu m$. Each crack length measurement was made twice to reduce measurement error, and each measurement was referenced to the root of the initial 0.50mm radius notch. Crack opening stress level was verified optically as in reference [12]. Stress intensity factors were calculated using geometry factors from reference [13].

In the case of the mode II crack closure free crack growth experiments a 220kN axial and 2250N-m torsional servohydraulic frame with hydraulic collet grips was used. The notched tubular specimens were precracked using a torsional periodic overload strain

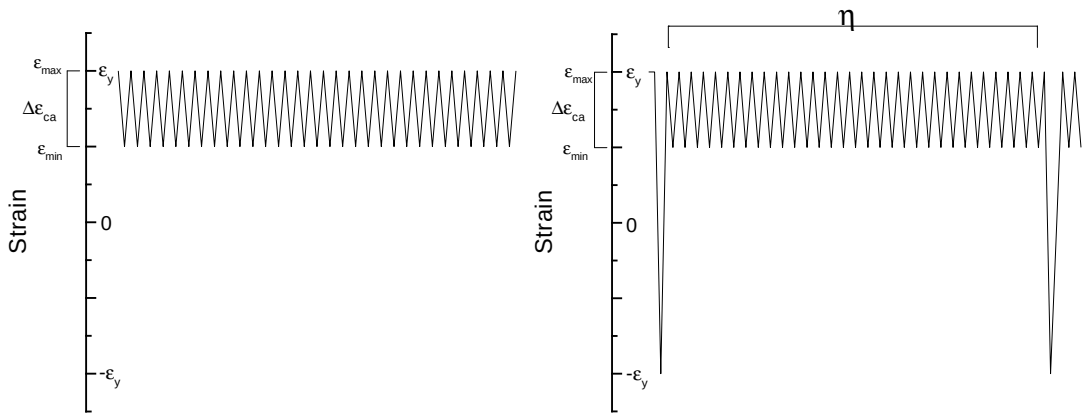

(a) Uniaxial Hi R-ratio history (b) Periodic Overload History

Figure 4. Load histories used in crack growth testing.

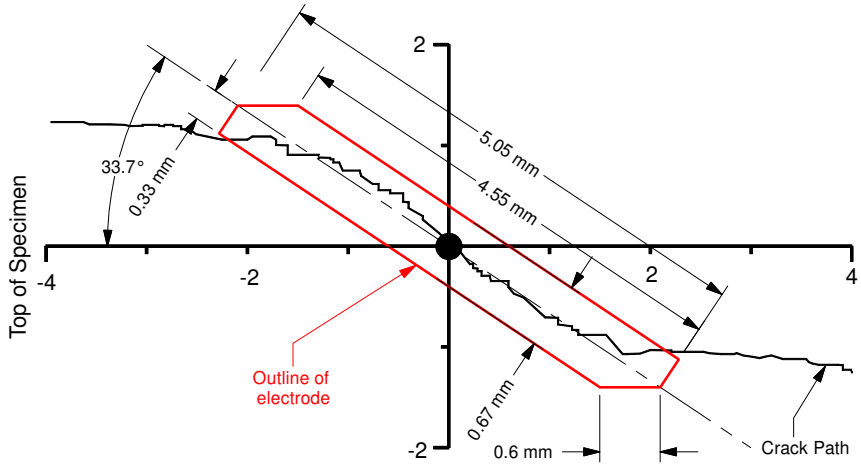

Figure 5. Example of electron discharge machining precrack removal.

history such as the one depicted in Figure 4b. Precracking was conducted under shear strain control (the axial force was held at 0) with the small cycle torsional strain amplitude ($(\varepsilon_{xy}^{sc})_a$) set at the constant amplitude fatigue limit (and $\eta = 100$). In this document the tensorial shear strain (ε_{xy}) is used rather than the engineering shear strain (γ_{xy}, where $\gamma_{xy} = 2\varepsilon_{xy}$). Dental impression material was used to verify that the crack had stabilized both in the inside and outside surfaces of the tube and that the crack lengths and paths were the same. The initial portion of the crack that grew on planes of maximum tension out of the notch (0.25mm hole) before switching on to the longitudinal shear plane was removed via plunge electron discharge machining using an electrode specifically designed for that specimen's crack, as in Figure 5. The removal eliminates asymmetric load transfer across this section of the crack during torsional loading. Complete removal was verified with dental impression material. Crack growth measurements were made with the same system and techniques as those used for mode I tests, but length measurements were made from crack tip to crack tip. Stress intensity calculations were made on the basis of the geometry factor found in reference [14]. For the purposes of the growth rate calculation

only longitudinal crack lengths measurements were used in stress intensity calculations since, after the initial precracking, the the great predominance of crack growth was in that direction (transverse crack growth was ignored).

All mode II crack growth testing was conducted with periodic overload histories. The overload was applied under strain control (fully reversed torsional overload strain, $((\varepsilon_{xy}^{ol})_a = 0.0035)$, but the small cycles were applied under torsion control. Identifying crack face interference-free crack growth behavior was complicated in these tests since the crack faces were observed to slide back and forth rather than together and apart as observed in mode I loading. In this case an overload level and η, the number of small cycles between overload applications, that caused growth during the smaller cycles to take place under fully interference-free conditions was determined in the following manner. For a given overload level and η small cycle growth rates were recorded, and a second test was run with the same small cycle size and η, but with a much higher overload amplitude level. If the second small cycle crack growth rate was the same as the first, the first overload level was presumed to have resulted in crack-face interference-free crack growth for this small cycle amplitude. It was also assumed that other lower small cycle amplitudes would also be crack face interference-free for the first overload level and η. As the small cycle size decreased, the number of small cycles between overloads (η) was periodically increased. At each increase in η, an extra crack length measurement was made at $\eta/2$. If the crack growth extension was the same for the first and second halves of the small cycle block then the cycle was assumed to still be crack face interference-free for that η.

Locating the crack tip in these tests was more difficult than in the mode I tests. Although a mode II crack is clearly visible typically to within $50\mu m$ of the tip (largely due to fretting debris), beyond this point the crack path and especially the crack tip become exceedingly difficult to identify. In mode I tests the crack tip is obvious since the crack visibly opens all the way to the tip at the peak tension level. The primary method of locating a mode II crack tip was through observation of the sliding crack faces along the crack path and the deformation field around the crack tip. In addition, on the specimen surface there are dark areas of intense local deformation into which the crack occasionally grows, making precise observations difficult. Finally, measurements were discarded when the crack bifurcated. In this case the crack was grown away from the bifurcation and crack growth measurements were started anew. These problems were exacerbated near the threshold stress intensity (below about $4\text{MPa}\sqrt{\text{m}}$) because the deformation field, and hence the crack tip, became less distinct. It is estimated that the scatter in the crack growth rate in the Paris region was roughly one order of magnitude and in the threshold region (below $4\text{MPa}\sqrt{\text{m}}$), it was up to two orders of magnitude.

RESULTS AND DISCUSSION

Four SEN specimens were used to generate the crack closure-free mode I crack growth data plotted in Figure 6a, and the term “uncorrected” in this figure refers to the fact that indicated overload cycles have not been corrected for closure. Note that ΔK_{eff} as used in

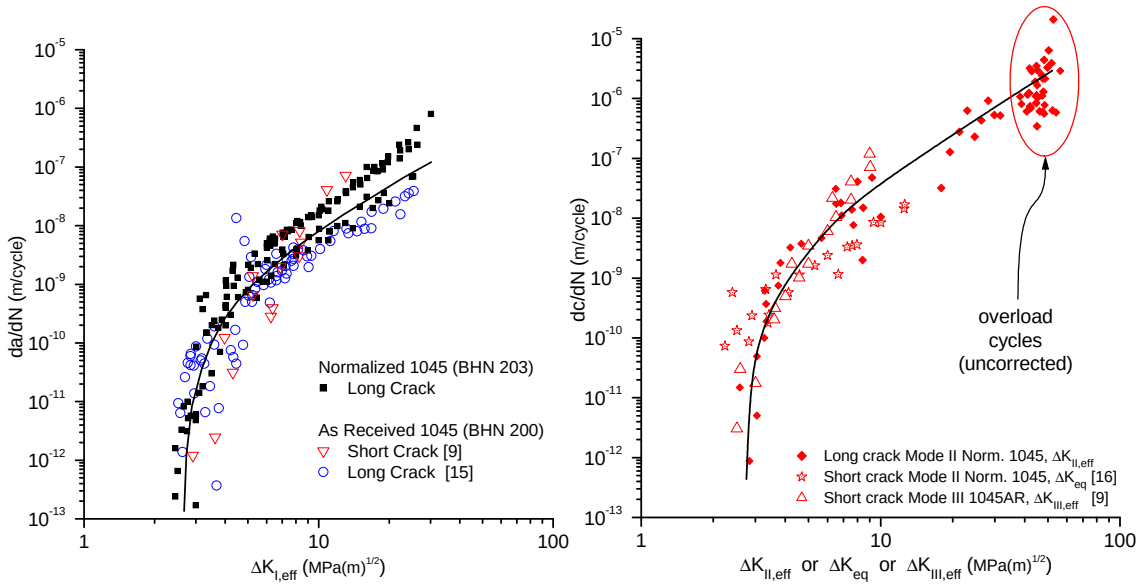

(a) Mode I effective crack growth rate curves (b) Mode II/III effective crack growth rate curves

Figure 6. Effective (Mode I crack closure free or Mode II/III crack-face interference-free) crack growth rate curves for normalized SAE 1045 steels.

this document refers the part of the stress-intensity cycle for which the crack is crack-face interference-free (or fully effective). It is not an equivalent stress intensity for mixed-mode crack growth (here, ΔK_{eq}) as is used sometimes in the literature.

The long crack data (solid squares) are self-consistent and agree with previous work by MacDougall and Topper [15] (open circles) on a very similar SAE 1045 AR steel. Further, this data agrees fairly well with data obtained by Varvani-Farahani and Topper [9], who used a confocal scanning laser microscope to directly measure the growth of 5-500μm cracks, for the same steel. This data is given by open down-triangles in Figure 6a. Lastly, in this figure it can be seen that both the long crack and the short crack mode I data fall into a consistent band, suggesting that, under fully open crack growth conditions, the long crack growth exhibits the same high crack growth rates that are observed for short and small cracks.

Two tubular crack growth specimens were used to obtain the crack-face interference-free growth data that is shown together with mode III short crack data from reference [9] in Figure 6b. Again, the long crack mode II crack-face interference-free crack growth data and the mode III short crack data fall into a fairly tight band. The similarity in the data sets implies that the crack growth rate under mode II and mode III are the same for this material.

All of the data sets are combined in Figure 7 where it is clear that the data for all three modes fall into a single band. This observation was also made by Socie, et al. [16] who studied short mode I and II fatigue cracks (20μm -1mm) in this same steel. Their measurements, made from acetate replicas, fall into the same scatter band and are shown in Figure 7.

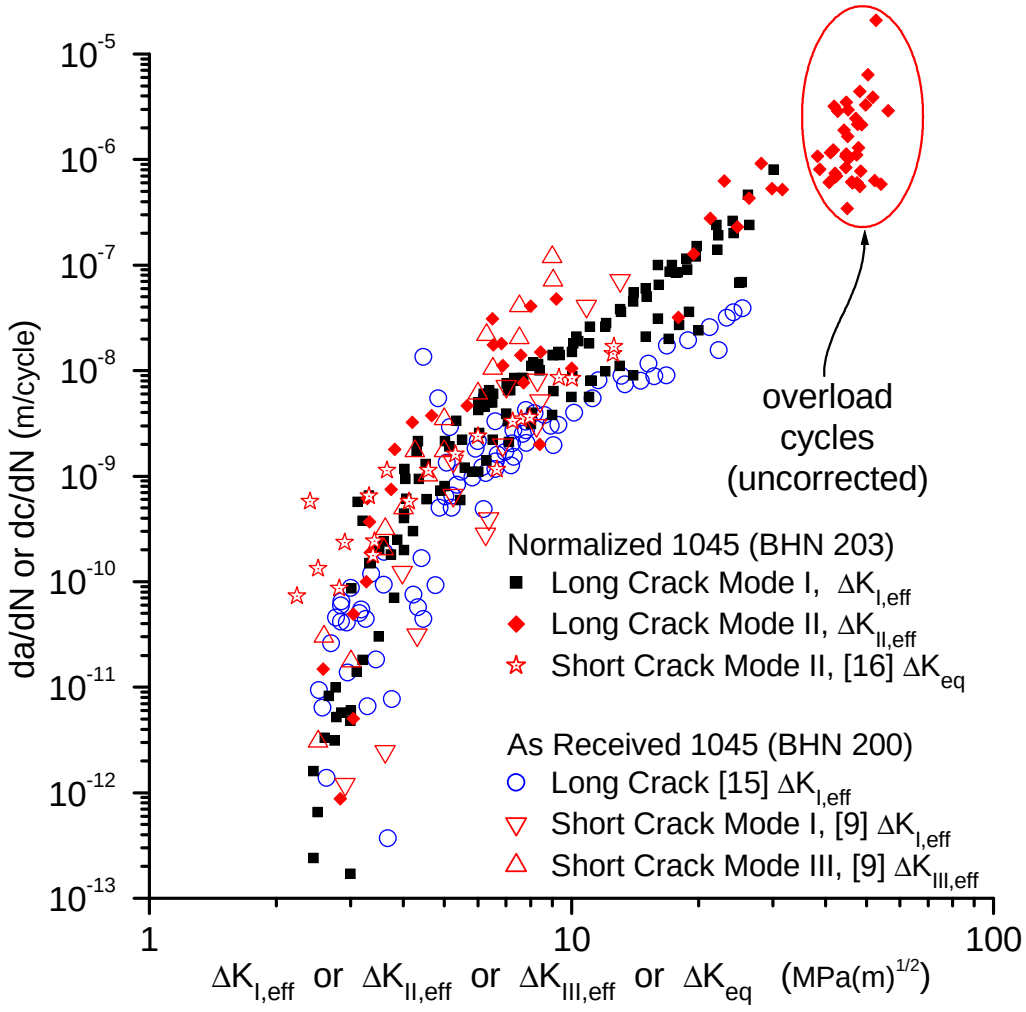

Figure 7. Mode I, mode II, and mode III effective crack growth rate data for soft SAE 1045 steels combined. Long crack mode I data from[15], short crack mode I and III data from [9], and mode II short crack data from [16].

The convergence of the long and short crack behavior in soft steels suggests that, once crack face interference is removed from crack growth in soft medium carbon steels, a single fatigue crack growth curve may be used to describe the fatigue crack growth behavior, for all crack growth modes or regimes (small, short, or long cracks).

CONCLUSIONS

1. A series crack of growth experiments were conducted on normalized SAE 1045 steel, and the crack closure-free fatigue crack growth rate data were determined for Mode I.

2. Special experimental techniques were developed to determine the crack-face interference-free Mode II crack growth rate data.
3. These curves were compared with other short crack or otherwise interference-free Mode I and Mode III crack growth data for similar steels taken from the literature, and it was found that the data fell into a single band for all crack growth modes for both long and short cracks.
4. The coincidence of the crack growth data bands was taken to indicate that a crack-face interference-free crack growth curve taken from one growth mode may be employed to predict crack growth for another loading mode.

REFERENCES

1. Elber, W. (1970). *Engineering Fracture Mechanics* **2**(1), 37–45.
2. Elber, W. (1971). In: *Dam. Tol. in Aircraft Struct.*, ASTM STP 486, pp. 230–242, Amer. Soc. Test. Mat., Phil.
3. DuQuesnay, D. L., Topper, T. H., Yu, M. T. and Pompetzki, M. A. (1992). *Int. J. Fat.* **14**(1), 45–50.
4. Hopper, C. and Miller, K. (1977). *Journal of Strain Analysis* **12**(1), 23–28.
5. Bonnen, J. J. F. and Topper, T. H. (1999). *Int. J. Fat.* **21**(1), 23–33.
6. Kaufman, R. P. and Topper, T. H. (2003). In: *Biax./Multiax. Fat. and Fract.*, ESIS STP 31, pp. 123–146. Elsevier Int. Ser. on Struct. Integ., 31, ISBN: 0-08-044129-7.
7. Jurcevic, R., DuQuesnay, D. L., Topper, T. H. and Pompetzki, M. A. (1990). *Int. J. Fat.* **12**(4), 259–266.
8. Bonnen, J. J. F. and Topper, T. H. (1999). In: *Multiax. Fat. & Deform.: Test. & Pred.*, Kalluri, S. and Bonacuse, P. J., eds., ASTM STP 1387, pp. 213–231, Amer. Soc. Test. Mat., Phil.
9. Varvani-Farahani, A. and Topper, T. H. (1999). *Fat. Frac. Eng. Mat. Struct.* **22**(8), 697–710.
10. Socie, D. and Leese, G. (Eds.) (1989). *Multiaxial Fatigue: Analysis and Experiment*, AE-14, Soc. of Automotive Engineers.
11. Cordes, T. and Lease, K. (Eds.) (1999). *Multiaxial Fatigue of an Induction Hardened Shaft*, AE-28, Soc. of Automotive Engineers, Warrendale, PA.
12. Dabayeh, A. A. and Topper, T. H. (1995). *Int. J. Fat.* **17**(4), 261–269.
13. Brown, W., Jr. and Srawley, J. (1966). In: *Plane Strain Crack Toughness Testing of High Strength Metallic Materials*, ASTM STP 410, p. 12, Amer. Soc. Test. Mat.
14. Lakshminarayana, H. and Murthy, M. (1976). *Int. J. Fract.* **12**, 547–566.
15. MacDougall, C. and Topper, T. H. (1997). *Int. J. Fat.* **19**(5), 389–400.
16. Socie, D., Hua, C. and Worthem, D. (1987). *Fat. Frac. Eng. Mat. Struct.* **10**(1), 1–16.